

## **Bottom-Up Synthesis of Crystalline Covalent Organic Framework Nanosheets, Nanotubes, and Kippah Vesicles: An Odd–Even Effect Induction**

Koner, K.; Sadhukhan, A.; Karak, S.; Sekhar Sasmal, H.; Ogaeri, Y.; Nishiyama, Y.; Zhao, S.; Polozij, M.; Kuc, A. B.; Heine, T.; Banerjee, R.;

Originally published:

June 2023

**Journal of the American Chemical Society 145(2023)26, 14475-14483**

DOI: <https://doi.org/10.1021/jacs.3c03831>

Perma-Link to Publication Repository of HZDR:

<https://www.hzdr.de/publications/Publ-37301>

Release of the secondary publication  
on the basis of the German Copyright Law § 38 Section 4.

# Bottom-up Synthesis of Crystalline Covalent Organic Framework Nanosheets and Nanotubes: An Odd-Even Effect Induction

Kalipada Koner,<sup>1,2\*</sup> Arnab Sadhukhan,<sup>1,2</sup> Himadri Sekhar Sasmal,<sup>1,2</sup> Suvendu Karak,<sup>1,2</sup> Yutaro Ogaeri,<sup>3,4</sup> Yusuke Nisiyama,<sup>3,4</sup> Shuangjie Zhao,<sup>5,6,7</sup> Miroslav Položij,<sup>5,6,7</sup> Agnieszka Kuc,<sup>5,6,7</sup> Thomas Heine,<sup>5,6,7</sup> and Rahul Banerjee<sup>1,2\*</sup>

<sup>1</sup>Department of Chemical Sciences, Indian Institute of Science Education and Research, Kolkata; Mohanpur 741246, India.

<sup>2</sup>Centre for Advanced Functional Materials, Indian Institute of Science Education and Research, Kolkata; Mohanpur 741246, India.

<sup>3</sup>RIKEN-JEOL Collaboration Center, RIKEN; Yokohama, Kanagawa, 230-0045, Japan

<sup>4</sup>JEOL RESONANCE Inc.; Musashino, Akishima, Tokyo, 196-8558, Japan.

<sup>5</sup>Faculty of Chemistry and Food Chemistry, Technische Universität Dresden, 01069 Dresden, Germany.

<sup>6</sup>Helmholtz-Zentrum Dresden-Rossendorf, Abteilung Ressourcenökologie, 04318 Leipzig, Germany.

<sup>7</sup>Department of Chemistry, Yonsei University and IBS Center for Nanomedicine, Seoul 03722, Republic of Korea.

\*Email: [kalipadagr@gmail.com](mailto:kalipadagr@gmail.com); [r.banerjee@iiserkol.ac.in](mailto:r.banerjee@iiserkol.ac.in), Tel: +033-6136-0000-1327, +033-6136-0000-1512.

---

**ABSTRACT:** Crystalline and porous few-layer organic nanosheets are becoming increasingly attractive as two-dimensional (2D) materials due to their precise atomic connectivity and tailor-made pores. However, most strategies for synthesizing nanosheets rely on surface-assisted methods and top-down exfoliation of stacked materials. To achieve the bulk-scale synthesis of 2D nanosheets with uniform size and crystallinity, a well-designed building block is necessary. We used reticular chemistry to synthesize crystalline covalent organic nanosheets (CONs) through Schiff base reactions between tetrapropylthianthrene tetraaldehyde (THT) and aliphatic diamines. The bent geometry of thianthrene in THT retards the out-of-plane stacking, while the flexible diamines introduce dynamic characteristics into the framework, facilitating nanosheet formation. Successful isoreticulation with five diamines with two to six carbon chain lengths generalizes the design strategy. Spectroscopic techniques, including advanced solid-state NMR and FTIR, established atomic-level connectivity between THT and diamines. Microscopic imaging reveals the odd-even effect of diamines on the post-transformation of CONs to nanotubes and hollow spheres. The single-crystal structure of repeating units indicates that the odd-even effect of diamines introduces irregular-regular curvature in the backbone, facilitating such dimensionality conversion. Theoretical calculations shed more light on nanosheet stacking and rolling behavior with even and odd diamines.

---

## INTRODUCTION

Covalent organic frameworks (COFs) are porous materials with highly ordered 2D or 3D networks constructed from organic building blocks.<sup>1,2</sup> These materials possess numerous desirable properties, such as structural adaptivity and predictability, large surface area, and extremely low density, making them highly attractive for various applications, including gas storage, separation, optoelectronics, and catalysis.<sup>3-5</sup> Recently, two-dimensional porous covalent organic nanosheets (CONs) have emerged as a new member in the family of 2D COFs with potential applications in chemical sensing, antimicrobial coatings, and cathode materials.<sup>6-11</sup> Current strategies for the preparation of CONs include top-down approaches, such as solvent-assisted exfoliation, self-exfoliation, mechanical delamination, or sequential post-synthetic modifications of COFs.<sup>12-15</sup> However, these strategies have limited success due to the layers' fragmentation, crystallinity loss during exfoliation. An alternative approach to control the thickness of COFs involves interface-confined growth, but this is difficult to scale up.<sup>16-22</sup> To address the challenges of exfoliating COFs, researchers have explored the use of weak interlayer linkages<sup>23-24</sup> or the introduction of bulky functionality like rotaxane in the COF backbone to allow easy exfoliation into monolayer sheets with well-defined

thicknesses.<sup>25</sup> However, the prepared CONs usually suffer from small domain sizes and large amounts of topological defects. The formation of fully developed 2D CONs requires precise control over the conformation of each building unit. Therefore, the bulk synthesis of crystalline CONs with a high aspect ratio demands a strategy that suppresses the growth in one dimension. This could be achieved by utilizing anisotropic crystal growth<sup>26</sup> or diminishing the layer stacking process.

We have introduced a bent thianthrene core and flexible aliphatic chains as building blocks to enhance the dynamic nature of individual COF layers, thereby restricting the interlayer  $\pi$ -stacking interactions. The Schiff base reaction between the thianthrene tetraaldehyde (THT) and linear aliphatic diamines at room temperature has resulted in the synthesis of porous, crystalline CONs at a bulk scale. We have successfully synthesized five CONs, namely, THTED, THTPrD, THBD, THTPnD, and THHD, using thianthrene tetraaldehyde (THT) and five different aliphatic diamines, namely, 1,2-diaminoethane (ED), 1,3-diaminopropane (PrD), 1,4-diaminobutane (BD), 1,5-diaminopentane (PnD), and 1,6-diaminohexane (HD), respectively, to generalize the synthetic design. The CONs synthesized with even aliphatic chains, such as THTED, THTBD, and THTHD, remain as 2D flexible nanosheets.

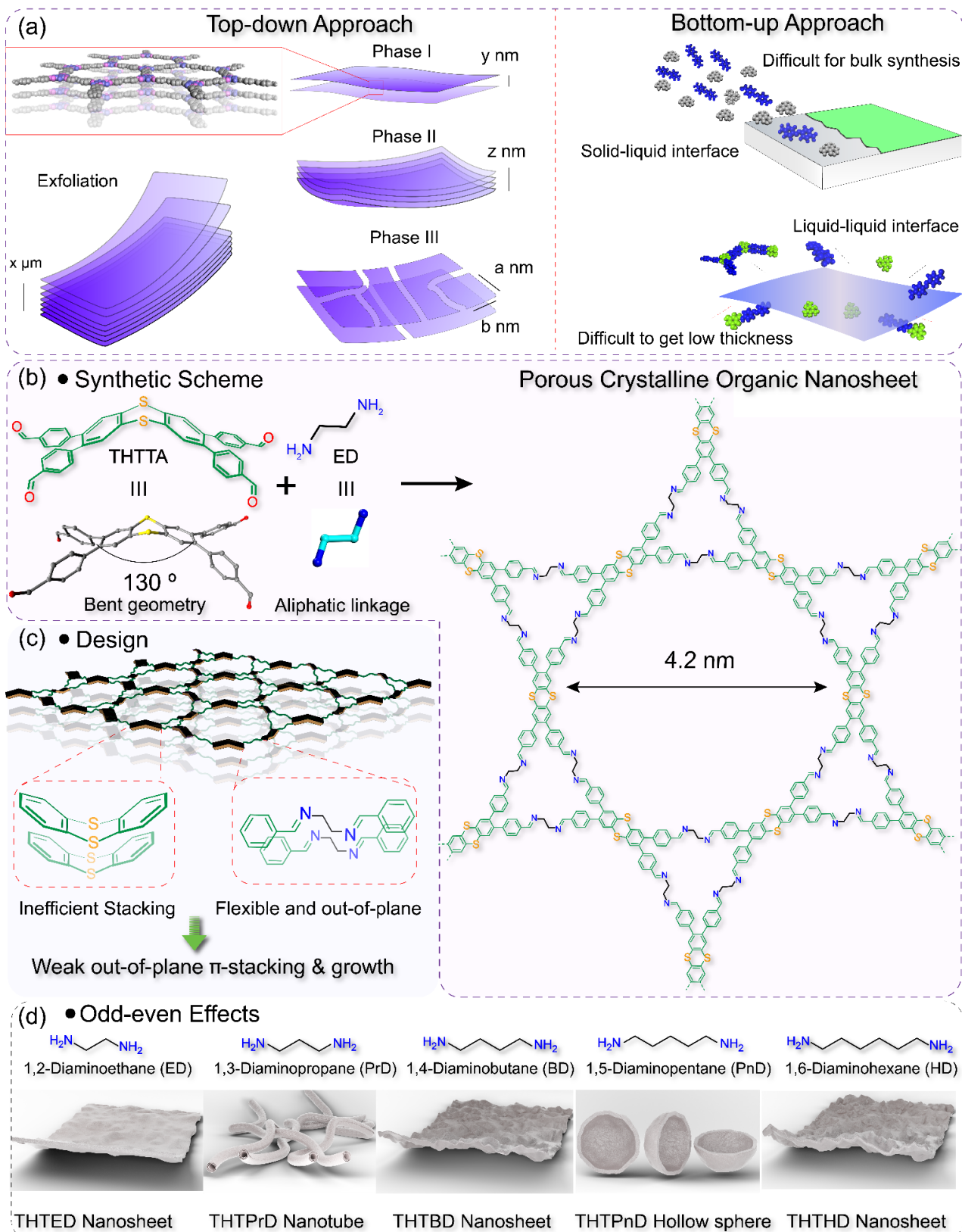


**Figure 1. Design of strategy and structure of Covalent Organic Nanosheets:** a) Previously reported methods, i.e., top-down and bottom-up approaches for synthesizing CONs. (b) Synthetic scheme of THTED CONs with starting material, i.e., thianthrene tetraaldehyde and 1,2 diaminoethane. (b) Bent geometry and the flexible nature of THTED CONs hinder efficient stacking. (d) The Odd-even effect of aliphatic linkers on the transformation of nanosheets to nanotubes, and hollow spheres.

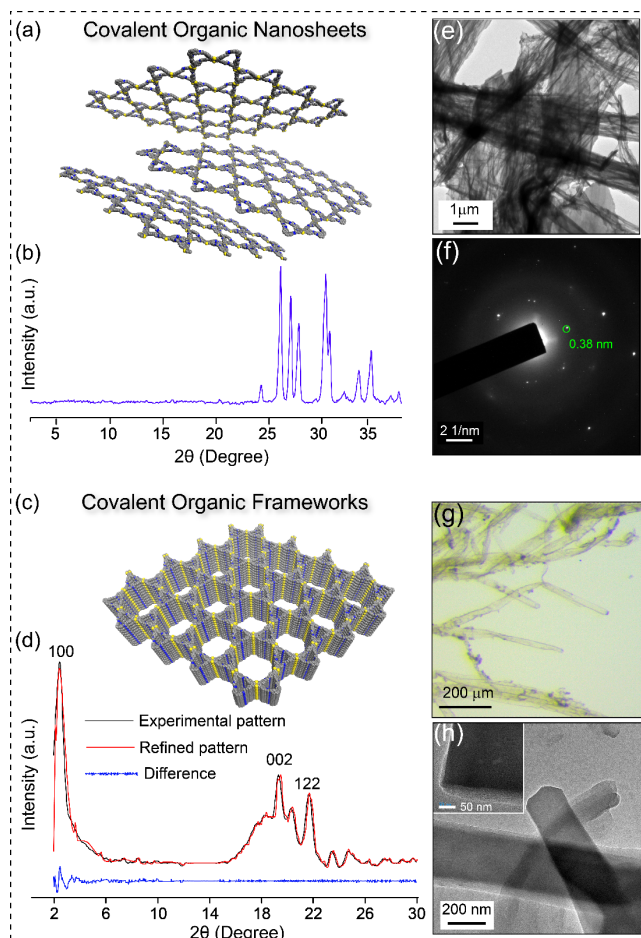


**Figure 2. Synthetic protocol and structural characterization of THTED CONs:** (a & c) A schematic representation of THTED CONs and stacked THTED COFs in the presence of DCM. (b & d) Powder X-ray diffraction (PXRD) pattern of dry THTED CONs and COFs in the presence of DCM along with Pawley refinement. (e & f) TEM image and selected area electron diffraction (SAED) of THTED CONs. (g) Optical image of THTED CONs in DCM. (h) TEM image of THTED COFs after direct drop casting from DCM solution (inset: zoomed section of stacked CONs).

On the other hand, the CONs synthesized with odd aliphatic chains, such as THTPrD and THTPnD, either roll into one-dimensional (1D) nanotubes or convert to hollow spheres (THTPnD). We further synthesized the repeating units of all COFs to gain further insight into the effects of odd-even aliphatic carbon atoms. Theoretical investigations of each nanostructure have shed more light on two categories of 2D nanosheets based on the odd-even effect.<sup>27-28</sup> Even diamines result in structures with regular sinus-like waves for THTED and THTBD, while odd diamines result in structures with irregular, double waves for THTPrD and THTPnD.

## RESULTS AND DISCUSSION

Our strategy for creating few-layer 2D covalent organic nanosheets (CONs) relies on modulating the planarity, rigidity, and reactivity of the building blocks by introducing bent geometry and flexibility in the linkers. Specifically, we have focused on utilizing a bent thianthrene-based tetraaldehyde, i.e., 4,4',4'',4'''-(thianthrene-2,3,7,8-tetrayl) tetrabenzaldehyde (THT) and flexible aliphatic diamines

such as 1,2-diaminoethane (ED), 1,3-diaminopropane (PrD), 1,4-diaminobutane (BD), 1,5-diaminopentane (PnD), and 1,6-diaminohexane (HD) to construct the few-layer 2D CONs (Figure 1). The dihedral angle of approximately 130° between two opposite terminal aldehyde ( $-\text{HC}=\text{O}$ ) groups of THT weakens the out-of-plane  $\pi$ -stacking interactions, as shown in Figure 1b. We anticipated that aliphatic diamines would enhance the dynamic nature between layers of 2D COFs and hinder efficient  $\pi$ -stacking (Figure 1c). Moreover, the higher nucleophilicity of aliphatic amines, in comparison to aromatic amines, should accelerate the in-plane (ab plane) growth of nanosheets.

We synthesized THTED via imine condensation reactions between 1 equivalent of THT (31.6 mg, 0.05 mmol) and 2 equivalent of 1,2-diaminoethane (ED) (6 mg, 0.1 mmol) (Figure S6). THT was dissolved in 100 ml of dry and degassed dichloromethane (DCM), and a solution of ED in 50 ml dry DCM was added dropwise into THT solution in the presence of 250  $\mu\text{L}$  glacial acetic acid at 0 °C. After 6 hours, spherulite-like nucleation of the CONs started on the wall of the flask (Figure S6), which grew with time. After 24 hours, one-dimensional growth led to the formation of millimeter-scale ( $>0.5$  mm) THTED CONs (Figure 2g). We collected the resulting yellowish-white material by filtration and washed it with anhydrous DCM and methanol. Then we dried it at 60 °C for 3 hours resulting in a yield of 24 mg of THTED (70% yield). We extended this design strategy to synthesize four more CONs using four diamines (Figure 1d). In the typical synthesis, a solution of 0.1 mmol 1,3-diaminopropane (PrD) (7.4 mg), 1,4-diaminobutane (BD) (8.8 mg), 1,5-diaminopentane (PnD) (10.2 mg) and 1,6-diaminohexane (HD) (11.6 mg) in 50 ml anhydrous DCM was separately added dropwise into a solution of 0.05 mmol THT (31.6 mg) in 100 ml DCM in the presence of catalytic acetic acid to yield THTPrD (18 mg, 51%), THTBD (14 mg, 38%), THTPnD (10 mg, 26%) and THTHD (27 mg, 68%) respectively (Supplementary section 1.3). We collected and dried each material following the same procedure as for THTED.

The powder X-ray diffraction (PXRD) pattern of THTED displays intense peaks between  $2\theta = 26.1^\circ$  to  $34.6^\circ$  (Figure 2b), which typically correspond to the reflections from planes parallel to the ab plane of 2D lattice in the  $2\theta$  range of 25 to  $35^\circ$ . The high-resolution transmission electron microscope (HRTEM) image reveals a uniform corrugated nanosheet structure for this material (Figure 2e). In the selected area electron diffraction (SAED) in HRTEM, the diffraction spots align with an interplanar distance of 0.38 nm, indicating the possible interlayer distance between individual (001) planes (Figure 2f). While both PXRD and SAED patterns suggest the crystalline nature of THTED CONs, simulating the structure of the CONs without information on the (100) planes is challenging. To obtain information about the diffraction patterns of the (100) planes, we collected the PXRD of the soaked THTED material (spherulite-like material in DCM) because the solvent (DCM) may assist in stacking these nanosheets and thereby recreate stacking of the (100) planes (Figure 2h).<sup>29</sup> The PXRD pattern of DCM soaked THTED sample reveals a peak at  $2\theta = 2.4^\circ$ , corresponding to reflections from the (100) planes (Figure 2d).



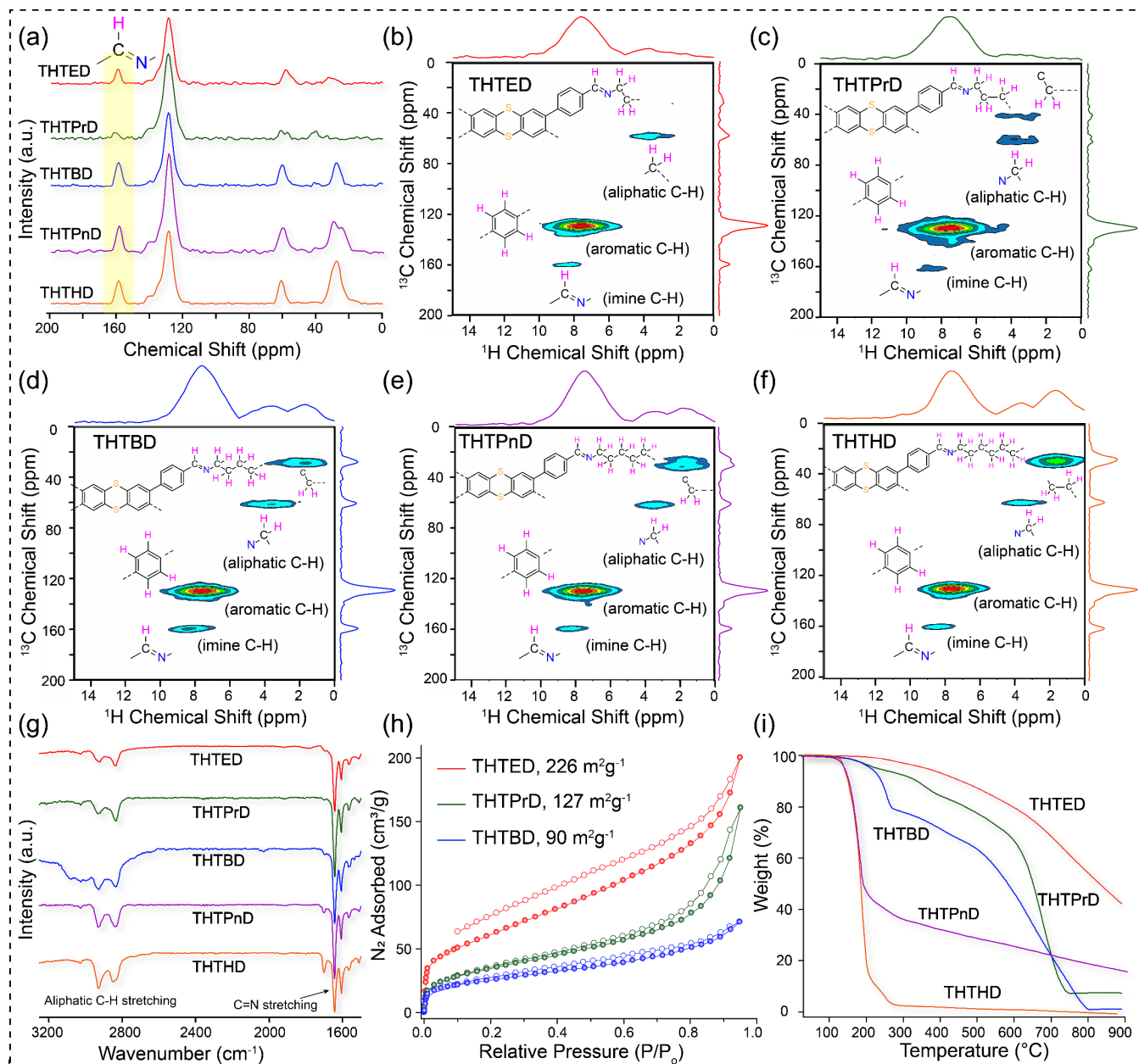


**Figure 3. Spectroscopic characterization and physical properties of all materials:** (a) The  $^{13}\text{C}$  projection of solid state two-dimensional (2D)  $^{13}\text{C}$ - $^1\text{H}$  correlation NMR of all the isorecticular frameworks. (b-f) 2D solid-state  $^{13}\text{C}$ - $^1\text{H}$  double cross-polarization (CP) correlation NMR of THTED, THTPrD, THTBD, THTPnD, and THTHD, respectively. (g) Fourier transformed infra-red (FTIR) spectra of all five materials showing intense peaks for imine ( $-\text{HC}=\text{N}-$ ) bond stretching at  $1643\text{ cm}^{-1}$ . (h)  $\text{N}_2$  adsorption isotherm for THTED, THTPrD, and THTBD shows declining BET surface area from THTED to THTBD. (i) Thermogravimetric analysis (TGA) for all the framework material.

To elucidate the structure of the THTED CONs and calculate unit cell parameters, we built two possible 2D models with rhombic square (sql) and Kagome (kgm) topology from THT and linear ED (Supplementary section 3).<sup>30</sup> The position of the first peak for (100) plane reflections in the experimental PXRD pattern aligns well with the simulated pattern of the Kagome lattice. We performed Pawley refinements for the THTED Kagome structure to find unit cell parameters, giving the values  $a=47.9\text{ \AA}$ ,  $b=47.5\text{ \AA}$ , and  $c=8.52\text{ \AA}$ . The THTED CONs consist of two types of pores, one  $4.2\text{ nm}$  pore surrounded by six  $1.6\text{ nm}$  pores (Figure 2c).

To determine the atomic level connectivity of these frameworks, we conducted solid-state 2D NMR analyses,

including  $^{13}\text{C}$ - $^1\text{H}$  correlation and  $^1\text{H}$ - $^1\text{H}$  double quantum-single quantum (DQ-SQ) NMR techniques. The  $^{13}\text{C}$ - $^1\text{H}$  correlation NMR technique only shows the covalently bonded C-H pairs under ultrafast MAS of  $70\text{ Hz}$ . We have also extracted 1D solid-state  $^{13}\text{C}$  NMR from the Y-axis projection of the  $^{13}\text{C}$ - $^1\text{H}$  correlation (Figure 3a). All CONs, namely THTED, THTPrD, THTBD, THTPnD, and THTHD, exhibit a distinct  $^{13}\text{C}$  peak at  $159.5$ ,  $161.5$ ,  $159.5$ ,  $160$ , and  $159.5\text{ ppm}$ , respectively. These peaks correspond to imine ( $-\text{HC}=\text{N}-$ ) carbons. The 2D  $^{13}\text{C}$ - $^1\text{H}$  correlation NMR provides further insight into imine ( $-\text{HC}=\text{N}-$ ) linkages and the aliphatic methylene carbons ( $-\text{CH}_2-$ ) in the backbone. THTED displays a prominent spot at  $8.6\text{ ppm}$  for  $^1\text{H}$  along X-

axis and 159.5 ppm for  $^{13}\text{C}$  along Y-axis { $^1\text{H}$ : 8.6 ppm,  $^{13}\text{C}$ : 159.5 ppm} corresponding to the imine ( $-\text{HC}=\text{N}-$ ) C–H groups and another prominent spot at 3.7 ppm for  $^1\text{H}$  along X-axis and 58.6 ppm for  $^{13}\text{C}$  along Y-axis { $^1\text{H}$ : 3.7 ppm,  $^{13}\text{C}$ : 58.6 ppm} for aliphatic methylene ( $-\text{CH}_2-$ ) groups (Figure 3b). The aromatic C–H correlation appears between aliphatic and imine ( $-\text{HC}=\text{N}-$ ) C–H from  $^{13}\text{C}$ : 124.5 ppm to  $^{13}\text{C}$ : 138 ppm. In THTPrD, in addition to the characteristic imine ( $-\text{HC}=\text{N}-$ ) signal at  $^1\text{H}$ : 8.5 ppm,  $^{13}\text{C}$ : 161.5 ppm, the two non-equivalent methylene ( $-\text{CH}_2-$ ) group appears at  $^1\text{H}$ : 2.8 ppm,  $^{13}\text{C}$ : 41.0 ppm and  $^1\text{H}$ : 3.6 ppm,  $^{13}\text{C}$ : 60.7 ppm (Figure 3c). The former methylene carbon ( $-\text{CH}_2-$ ) signal in THTPrD is less intense than the latter since the ratio of two aliphatic C–H is 2:1. Similarly, THTBD displays three signals with comparable intensities aside from the aromatic region (Figure 3d). The signal at  $^1\text{H}$ : 8.3 ppm,  $^{13}\text{C}$ : 159.5 ppm corresponds to the imine C–H correlation. The other signals in the aliphatic region at  $^1\text{H}$ : 1.94 ppm,  $^{13}\text{C}$ : 28.3 ppm, and  $^1\text{H}$ : 3.7 ppm,  $^{13}\text{C}$ : 60.9 ppm correspond to two non-equivalent methylene ( $-\text{CH}_2-$ ) groups of butane chain. The equal intensity of these peaks is a result of the same ratio of imine ( $-\text{HC}=\text{N}-$ ), and two types of methylene ( $-\text{CH}_2-$ ) groups (1:1:1). When compared to the deshielded methylene ( $-\text{N}-\text{CH}_2-$ ) signal at  $^1\text{H}$ : 3.3 ppm,  $^{13}\text{C}$ : 61.5 ppm, the relative intensities of aliphatic shielded methylene ( $-\text{C}-\text{CH}_2-\text{C}-$ ) signals for THTPnD and THTHD at  $^1\text{H}$ : 1.94 ppm,  $^{13}\text{C}$ : 29.2 ppm are higher as the ratios of these two types of protons are 2:3 and 2:4 respectively (Figure 3e,f). In addition to the aliphatic signals, THTPnD and THTHD also exhibit signals for imine ( $-\text{HC}=\text{N}-$ ) C–H at  $^1\text{H}$ : 8.5 ppm,  $^{13}\text{C}$ : 159.5 ppm (Figure 3e, f). None of these CONs show any signal at  $^1\text{H}$ :  $\sim 10$  ppm,  $^{13}\text{C}$ :  $\sim 180$  ppm, indicating the absence of unreacted aldehyde ( $-\text{HC}=\text{O}$ ) groups. To further confirm the absence of aldehyde ( $-\text{HC}=\text{O}$ ) functionalities, we conducted solid-state  $^1\text{H}$ - $^1\text{H}$  DQ-SQ correlation NMR for THTED, THTPrD, THTBD, THTPnD, and THTHD (Figures S19, S26, S34, S40, and S47). The absence of any peak at SQ  $^1\text{H}$ :  $\sim 10$  ppm in all materials rules out the presence of aldehyde ( $-\text{HC}=\text{O}$ ) groups. The 1D and 2D NMR confirm the complete conversion to imine ( $-\text{HC}=\text{N}-$ ) linkage between THT tetraaldehyde and aliphatic diamines. ATR-IR further supports the NMR results by exhibiting a sharp peak at  $1640\text{ cm}^{-1}$  for all CONs, corresponding to imine ( $-\text{HC}=\text{N}-$ ) stretching (Figure 3g). The intensity of aliphatic C–H stretching at  $3000\text{ cm}^{-1}$  also increases from THTED to THTHD in accordance with an increasing number of carbons in the aliphatic chain.

Although the overall atomic connectivity remains almost constant with an increase in the length of alkyl diamine, the dynamic nature and flexibility of the framework increase from THTED to THTHD, leading to a loss of crystallinity. This increased flexibility is evident in the  $\text{N}_2$  adsorption isotherms at 77 K, as shown in Figure 3h. THTED exhibits a type-II adsorption isotherm with a BET surface area of  $226\text{ m}^2\text{g}^{-1}$  (Figure S20). The BET surface area gradually decreases from THTED to THTPrD ( $127\text{ m}^2\text{g}^{-1}$ ) and eventually reaches its lowest point for THTBD ( $90\text{ m}^2\text{g}^{-1}$ ), while THTPnD and THTHD are nonporous (Figure S27, S35, S41, S48). The pore size distribution calculated using nonlocal density functional theory (NLDFT) of THTED, THTPrD, and THTBD exhibits two peaks at 1.6 and  $\sim 4.0$  nm.

The distribution with a higher pore volume at 1.6 nm corresponds to smaller trigonal pores, while the broad distribution at 4.0 nm indicates the large hexagonal pore of the kgm topology (Figure S20). THTPrD also shows broad distributions in the 15 to 25 nm range, which may be attributed to mesopore channels (Figure S27). In addition to the surface area, thermal stability decreases with an increasing chain length from THTED to THTPnD. Thermogravimetric analysis (TGA) of THTED under  $\text{N}_2$  atmosphere indicates a thermal stability of  $240\text{ }^\circ\text{C}$ , whereas THTPrD and THTBD are thermally stable up to  $200\text{ }^\circ\text{C}$ . THTPnD and THTHD are the least thermally stable among the five materials ( $170\text{ }^\circ\text{C}$ ) (Figure 3i).

Scanning electron microscopy (SEM) images of THTED show the flexible and corrugated nanosheets (Figure 4). HRTEM also supports the nanosheet morphology (Figure 4c). The height profile from the topographic images of atomic force microscopy (AFM) provides the thickness of THTED CONs of  $\sim 20$  nm (Figure 4d). Similar to THTED, the SEM images of THTBD show nanosheet morphology, although with shorter lengths ( $20\text{--}50\text{ }\mu\text{m}$ ) (Figure 4j). Uniform nanosheet structure is observed in TEM micrographs (Figure 4k), and the AFM topographic images support the nanosheet morphology with a thickness of  $\sim 5.1$  nm (Figure 4l). For THTHD, SEM, TEM, and AFM reveal a non-uniform nanosheet morphology due to the high flexibility of HD amines (Figure 4r–t). Due to their flexible and corrugated nature, all the nanosheets have an inherent tendency to roll (Figure S21–22). However, the rolling tendency increases significantly for THTPrD and converts the nanosheets to nanotubes like graphene to the carbon nanotube.<sup>31</sup> The SEM images of THTPrD show tubular morphology, with an average outer diameter of  $50 (\pm 10)$  nm and length of  $10\text{--}30\text{ }\mu\text{m}$  (Figure 4f, Figure S28). HRTEM micrographs of THTPrD show the nanotubes' uniform inner diameter of  $20 (\pm 5)$  nm (Figure 4g). The height profiles of THTPrD nanotubes from AFM reveal an outer diameter of  $50 (\pm 5)$  nm (Figure 4h, Figure S31). Surprisingly, THTPnD shows zero-dimensional (0D) hollow sphere morphology with  $0.5\text{--}1.5\text{ }\mu\text{m}$  diameter in SEM (Figure 4n). HRTEM micrograph reveals more information about the hollow spheres of  $0.4$  to  $1.4\text{ }\mu\text{m}$  inner diameter with  $100\text{--}150$  nm thick nanosheets-stacked wall (Figure 4o). As the growth of THTPrD nanosheets is small, the assembly of these nanosheets might result in hollow spheres rather than nanotubes.<sup>32</sup> Microscopic images reveal a correlation between even and odd numbers of carbon atoms of diamine and resultant materials. Diamines with even carbon atoms (THTED, THTBD, and THTHD) result in nanosheets material, while diamines with odd carbon atoms further transform the nanosheets to curved material like nanotubes (THTPrD) and hollow spheres (THTPnD). The thickness of the nanosheets decreases with increasing chain length as the enhancement of flexibility render stacking.

To investigate the odd-even effect in more detail, we synthesized the corresponding repeating units of THTED, THTPrD, THTBD, THTPnD, and THTHD CONs by reacting 4-(thianthren-2-yl)benzaldehyde with ED, PD, BD, PnD, and HD, respectively (Figure 5a, Supplementary section S2). The single crystal structure of the THTED monomer shows a linear connection between two thianthrene units with a

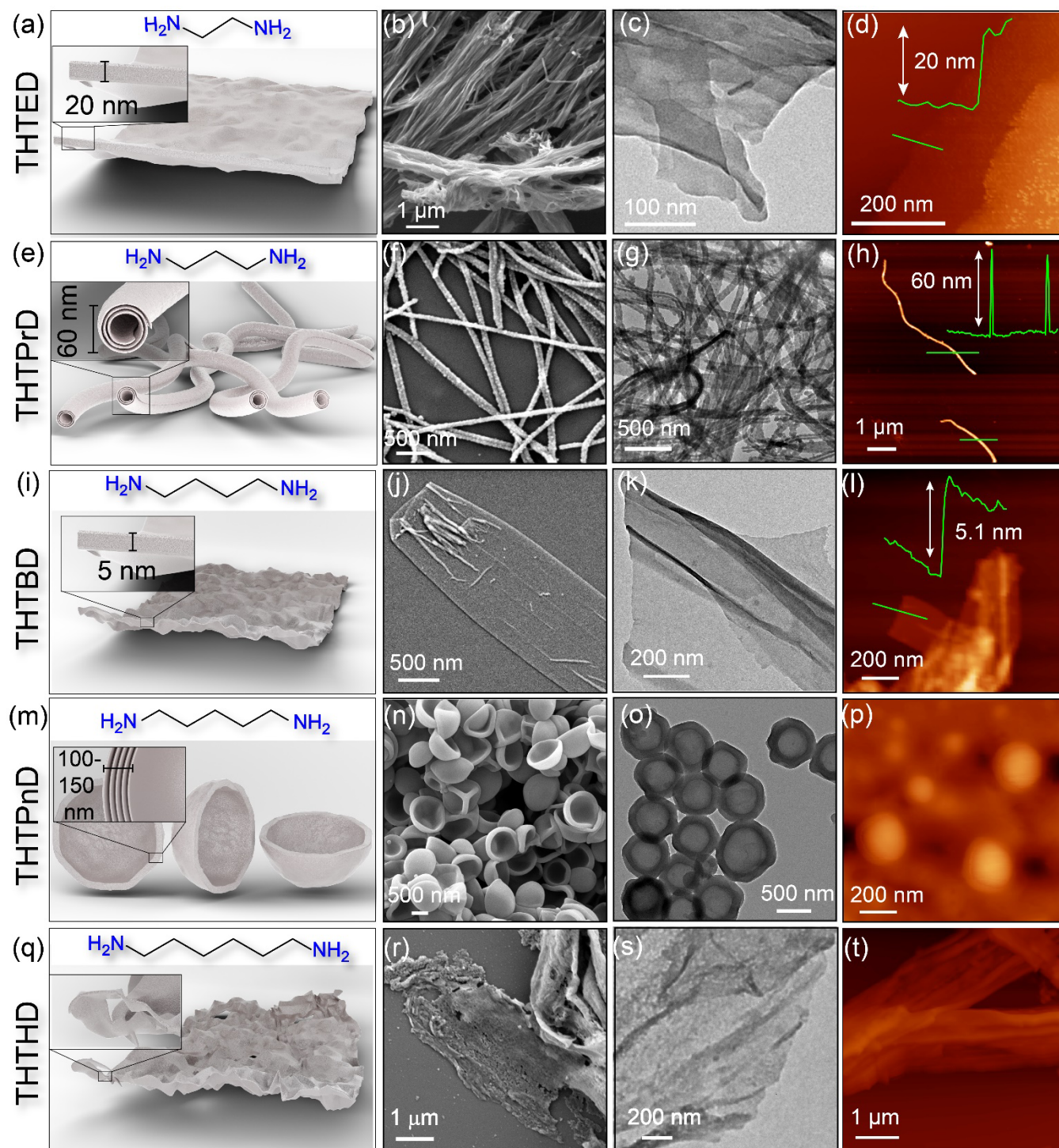


**Figure 4. Odd-even effect on the flexible two-dimensional nanosheets:** (a-d) The schematic representation, SEM image, TEM micrograph, and AFM image of THTED CONs. (e-h) The schematic representation, SEM image, TEM micrograph, and AFM image of the THTPrD nanotubes. (i-l) The schematic representation, SEM image, TEM micrograph, and AFM image of THTBD nanosheets. (m-p) The schematic representation, SEM image, TEM micrograph, and AFM image of the THTPnD hollow spheres. (q-t) The schematic representation, SEM image, TEM micrograph, and AFM image of THTHD nanosheets.

thianthrene-to-thianthrene angle of  $171^\circ$ . In contrast, the odd number of carbon atoms in THTPrD leads to in-plane curvature with an angle of  $130^\circ$ , resulting in two transimine bonds ( $-\text{HC}=\text{N}-$ ) with two thianthrene units (Figure 5b). The two thianthrene cores are linked again via a linear trans-bisimine ( $-\text{HC}=\text{N}-$ ) linkage with an angle of  $170^\circ$  for the THTBD monomer due to the even number of carbon atoms in BD diamine. This odd-even effect is also apparent in

the unit cell of THTED, THTPrD, and THTBD monomers. The THTED and THTBD monomers (even) adopt a centrosymmetric  $P2_1/c$  and  $P2_1/n$  space group, respectively, while the THTPrD (odd) crystallizes in a chiral  $P2_1$  space group (Supplementary section S8).

To explain the specific curling behavior of THTPrD and THTPnD, we modeled the geometric behavior of the five flexible CONs, as shown in Figure S57. To fully describe



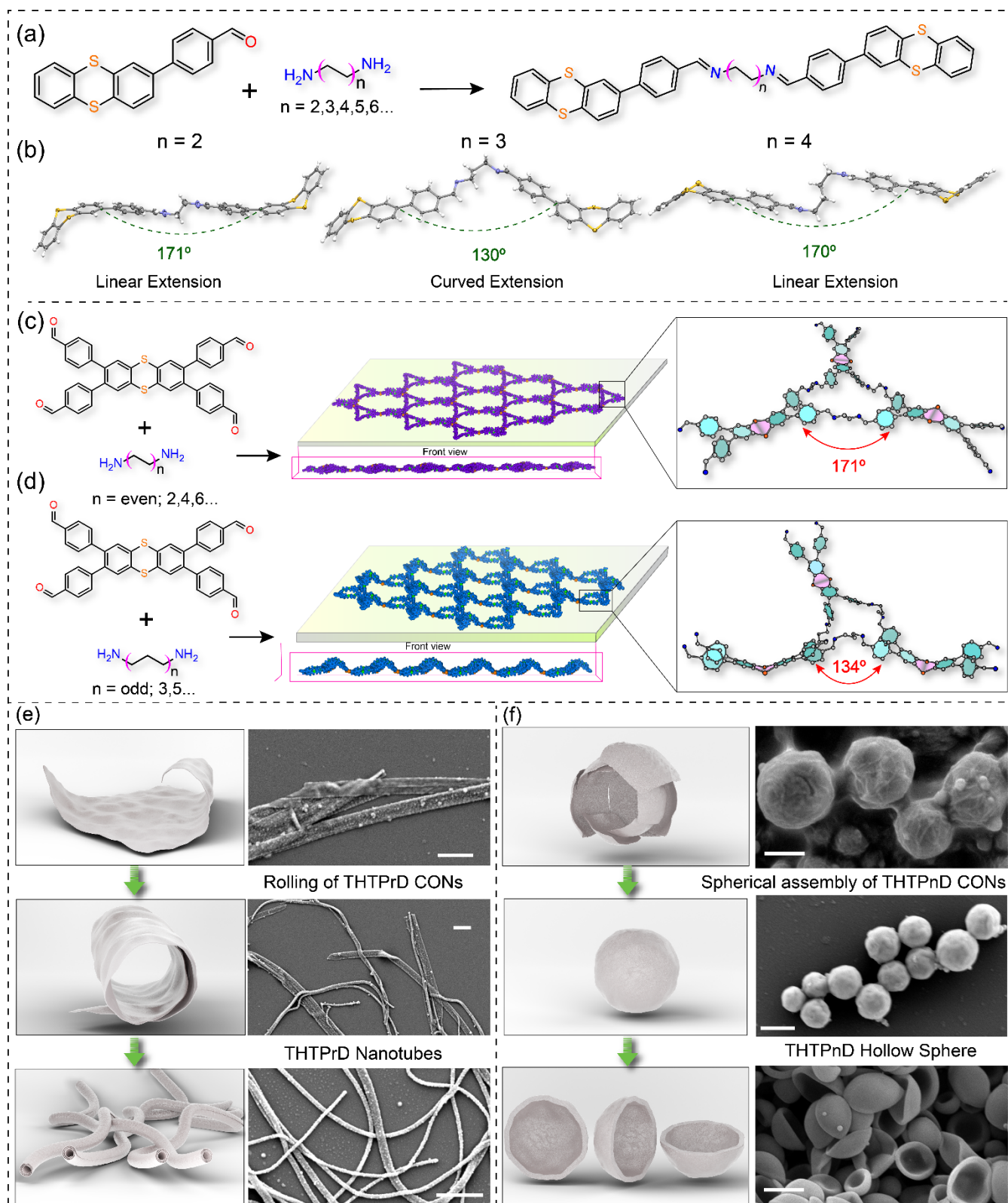


**Figure 5. Odd-even effect of diamines on the monomers and the framework material.** (a) Synthetic scheme of monomer preparation with varying diamine lengths from 2 to 6. (b) Single crystal structure of THTED, THTPrD, and THTBD along with unit cell parameters (below each crystal structure). (c & d) Geometry and energy-optimized (by SCC-DFTB 3 via DFTB+ and AMS, using Slater-Koster parameters (3ob-3-1)) structure of THTED and THTPrD nanosheets. (e & f) Detailed SEM studies of different phase of THTPrD nanotubes and THTPnD hollow sphere formation.

the layer corrugation, we used various unit cell sizes, including 2x2, 4x4, and 6x6, as larger layers allow for greater variation in the corrugation. However, we found that the

2x2 supercell was sufficient to describe the corrugation of the monolayer. The most significant structural characteristic of the CONs is their layer corrugation which



allows for their classification into two groups. The first group includes structures with regular sinus-like waves, such as THTED and THTBD. The second group includes structures with irregular double waves, such as THTPrD, THTPnD, and THTHD. The irregular waves observed in THTHD are mainly due to the high flexibility of the hexane chain. The different groups exhibit varying degrees of curvature (Figure X3), with THTED and THTBD displaying a curvature of approximately 140° (Figure 5C), while THTPrD and THTPnD exhibit curvatures ranging between 85° to 125° (Figure 5d). The acute angle created by these variations in surface constraints may impose surface constraints, which possibly cause THTPrD and THTPnD to roll, eventually forming nanotubes and hollow spheres. Detailed SEM studies of different phases of THTPrD nanotubes and THTPnD hollow sphere formation further support this phenomenon. The rolling of the THTED nanosheet results in nanotubes, whereas the THTPnD nanosheets assemble spherically and eventually form hollow spheres which further squeezed upon drying.

## CONCLUSION

In conclusion, we have developed a strategy to disrupt the out-of-plane  $\pi$ -stacking in two-dimensional COFs by incorporating bent and flexible aliphatic chains in the building blocks. These pre-designed building units enable the efficient bulk synthesis of few-layer crystalline, uniform, organic nanosheets, which is a marked improvement over surface-assisted growth and exfoliation of stacked 2D COFs. To generalize this design strategy, we have also developed five isorecticular frameworks. Solid-state NMR studies, including 2D  $^{13}\text{C}$ - $^1\text{H}$  double CP correlation NMR and  $^1\text{H}$ - $^1\text{H}$  DQ-SQ NMR, establish the atomic level connectivity for all five CONs. Microscopic imaging, including SEM, HRTEM, and AFM, reveals the odd-even effect on covalent organic nanosheets, which has remained largely unexplored in polymeric materials. The THTPrD nanosheets exhibit rolling behaviour along their edges to form one-dimensional nanotubes, similar to graphene to the carbon nanotube, providing a bottom-up synthetic strategy to make one-dimensional nanotubes without any template. The structure-morphology relationship has been established through detailed theoretical calculations of all the materials and the single-crystal structure of corresponding repeating units. We believe this design strategy has the potential to enable the production of several organic nanosheets and nanotubes in bulk without the need for surface or template support.

## ASSOCIATED CONTENT

Supporting Information. Synthesis, crystallography, and characterization details are provided in the Supporting Information file. This material is available free of charge via the Internet at <http://pubs.acs.org>.

## AUTHOR INFORMATION

Corresponding Author

\* [kalipadkr@gmail.com](mailto:kalipadkr@gmail.com)

\* [r.banerjee@iiserkol.ac.in](mailto:r.banerjee@iiserkol.ac.in)

## ORCID

Kalipada Koner: 0000-0002-9861-2712  
Arnab Sadhukhan: 0009-0009-4996-4592  
Yutaro Ogaeri: 0000-0002-0814-1698  
Yusuke Nishiyama: 0000-0001-7136-1127  
Shuangjie Zhao:  
Miroslav Položij:  
Agnieszka Kuc:  
Thomas Heine:  
Rahul Banerjee: 0000-0002-3547-4746

## Notes

The authors declare no competing financial interests.

## ACKNOWLEDGMENTS

K. K. acknowledges UGC for the research fellowship, A. S. acknowledges INSPIRE fellowship, R. B. acknowledges DST-Swarna Jayanti Fellowship grant (DST/SJF/CSA-02/2016-2017), DST Mission Innovation [DST/TM/EWO/MI/CCUS/17 DST/TMD(EWO)/IC5-2018/01(C)], SERB [CRG/2018/000314] and SERB SUPRA [SPR/2021/000020] for funding. Y.N. acknowledges the support of JSPS KAKENHI Grant Number 20K05483 and the JST-Mirai Program (Grant No. JPMJMI17A2, Japan).

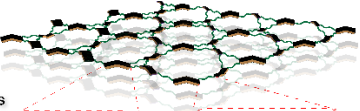
## REFERENCES

1. Cote, A. P.; Benin, A. I.; Ockwig, N. W.; O'Keeffe, M.; Matzger, A. J.; Yaghi, O. M., Porous, crystalline, covalent organic frameworks. *Science* **2005**, *310* (5751), 1166-70.
2. Diercks, C. S.; Yaghi, O. M., The atom, the molecule, and the covalent organic framework. *Science* **2017**, *355* (6328).
3. Lyu, H.; Diercks, C. S.; Zhu, C.; Yaghi, O. M., Porous Crystalline Olefin-Linked Covalent Organic Frameworks. *J. Am. Chem. Soc.* **2019**, *141* (17), 6848-6852.
4. Evans, A. M.; Parent, L. R.; Flanders, N. C.; Bisbey, R. P.; Vitaku, E.; Kirschner, M. S.; Schaller, R. D.; Chen, L. X.; Gianneschi, N. C.; Dichtel, W. R., Seeded growth of single-crystal two-dimensional covalent organic frameworks. *Science* **2018**, *361* (6397), 52-57.
5. Kandambeth, S.; Dey, K.; Banerjee, R., Covalent Organic Frameworks: Chemistry beyond the Structure. *J. Am. Chem. Soc.* **2019**, *141* (5), 1807-1822.
6. Chen, H.; Tu, H.; Hu, C.; Liu, Y.; Dong, D.; Sun, Y.; Dai, Y.; Wang, S.; Qian, H.; Lin, Z.; Chen, L., Cationic Covalent Organic Framework Nanosheets for Fast Li-Ion Conduction. *J. Am. Chem. Soc.* **2018**, *140* (3), 896-899.
7. Wang, S.; Wang, Q.; Shao, P.; Han, Y.; Gao, X.; Ma, L.; Yuan, S.; Ma, X.; Zhou, J.; Feng, X.; Wang, B., Exfoliation of Covalent Organic Frameworks into Few-Layer Redox-Active Nanosheetss as Cathode Materials for Lithium-Ion Batteries. *J. Am. Chem. Soc.* **2017**, *139* (12), 4258-4261.
8. Dong, J.; Zhang, K.; Li, X.; Qian, Y.; Zhu, H.; Yuan, D.; Xu, Q.-H.; Jiang, J.; Zhao, D., Ultrathin two-dimensional porous organic nanosheets with molecular rotors for chemical sensing. *Nat. Commun.* **2017**, *8* (1), 1142.
9. Wang, Q. H.; Kalantar-Zadeh, K.; Kis, A.; Coleman, J. N.; Strano, M. S., Electronics and optoelectronics of two-dimensional transition metal dichalcogenides. *Nat. Nanotech.* **2012**, *7* (11), 699-712.
10. Lin, Y. M.; Dimitrakopoulos, C.; Jenkins, K. A.; Farmer, D. B.; Chiu, H. Y.; Grill, A.; Avouris, P., 100-GHz Transistors from Wafer-Scale Epitaxial Graphene. *Science* **2010**, *327* (5966), 662-662.

11. Sun, B.; Kim, Y.; Wang, Y.; Wang, H.; Kim, J.; Liu, X.; Lee, M., Homochiral porous nanosheets for enantiomer sieving. *Nat. Mater.* **2018**, *17* (7), 599-604.
12. Berlanga, I.; Ruiz-Gonzalez, M. L.; Gonzalez-Calbet, J. M.; Fierro, J. L.; Mas-Balleste, R.; Zamora, F., Delamination of layered covalent organic frameworks. *Small* **2011**, *7* (9), 1207-11.
13. Coleman, J. N.; Lotya, M.; O'Neill, A.; Bergin, S. D.; King, P. J.; Khan, U.; Young, K.; Gaucher, A.; De, S.; Smith, R. J.; Shvets, I. V.; Arora, S. K.; Stanton, G.; Kim, H. Y.; Lee, K.; Kim, G. T.; Duesberg, G. S.; Hallam, T.; Boland, J. J.; Wang, J. J.; Donegan, J. F.; Grunlan, J. C.; Moriarty, G.; Shmeliov, A.; Nicholls, R. J.; Perkins, J. M.; Grievson, E. M.; Theuwissen, K.; McComb, D. W.; Nellist, P. D.; Nicolosi, V., Two-dimensional nanosheets produced by liquid exfoliation of layered materials. *Science* **2011**, *331* (6017), 568-71.
14. Khayum, M. A.; Kandambeth, S.; Mitra, S.; Nair, S. B.; Das, A.; Nagane, S. S.; Mukherjee, R.; Banerjee, R., Chemically Delaminated Free-Standing Ultrathin Covalent Organic Nanosheets. *Angew. Chem. Int. Ed.* **2016**, *55* (50), 15604-15608.
15. Mitra, S.; Kandambeth, S.; Biswal, B. P.; Khayum, M. A.; Choudhury, C. K.; Mehta, M.; Kaur, G.; Banerjee, S.; Prabhune, A.; Verma, S.; Roy, S.; Kharul, U. K.; Banerjee, R., Self-Exfoliated Guanidinium-Based Ionic Covalent Organic Nanosheets (iCONs). *J. Am. Chem. Soc.* **2016**, *138* (8), 2823-8.
16. Dai, W.; Shao, F.; Szczerbinski, J.; McCaffrey, R.; Zenobi, R.; Jin, Y.; Schluter, A. D.; Zhang, W., Synthesis of a Two-Dimensional Covalent Organic Monolayer through Dynamic Imine Chemistry at the Air/Water Interface. *Angew. Chem. Int. Ed.* **2016**, *55* (1), 213-7.
17. Zhou, D.; Tan, X.; Wu, H.; Tian, L.; Li, M., Synthesis of C-C Bonded Two-Dimensional Conjugated Covalent Organic Framework Films by Suzuki Polymerization on a Liquid-Liquid Interface. *Angew. Chem. Int. Ed.* **2019**, *58* (5), 1376-1381.
18. Liu, X.-H.; Guan, C.-Z.; Ding, S.-Y.; Wang, W.; Yan, H.-J.; Wang, D.; Wan, L.-J., On-Surface Synthesis of Single-Layered Two-Dimensional Covalent Organic Frameworks via Solid-Vapor Interface Reactions. *J. Am. Chem. Soc.* **2013**, *135* (28), 10470-10474.
19. Dey, K.; Pal, M.; Rout, K. C.; Kunjattu H, S.; Das, A.; Mukherjee, R.; Kharul, U. K.; Banerjee, R., Selective Molecular Separation by Interfacially Crystallized Covalent Organic Framework Thin Films. *J. Am. Chem. Soc.* **2017**, *139* (37), 13083-13091.
20. Liu, K.; Qi, H.; Dong, R.; Shivhare, R.; Addicoat, M.; Zhang, T.; Sahabudeen, H.; Heine, T.; Mannsfeld, S.; Kaiser, U.; Zheng, Z.; Feng, X., On-water surface synthesis of crystalline, few-layer two-dimensional polymers assisted by surfactant monolayers. *Nat. Chem.* **2019**, *11* (11), 994-1000.
21. Hao, Q.; Zhao, C.; Sun, B.; Lu, C.; Liu, J.; Liu, M.; Wan, L. J.; Wang, D., Confined Synthesis of Two-Dimensional Covalent Organic Framework Thin Films within Superspreading Water Layer. *J. Am. Chem. Soc.* **2018**, *140* (38), 12152-12158.
22. Chen, C.; Joshi, T.; Li, H.; Chavez, A. D.; Pedramrazi, Z.; Liu, P. N.; Li, H.; Dichtel, W. R.; Bredas, J. L.; Crommie, M. F., Local Electronic Structure of a Single-Layer Porphyrin-Containing Covalent Organic Framework. *ACS Nano* **2018**, *12* (1), 385-391.
23. Desiraju, G. R.; Steiner, T. The Weak Hydrogen Bond in Structural Chemistry and Biology. *IUCr Monographs on Crystallography*; Oxford, Oxford University Press/International Union of Crystallography, 1999; Vol. 9.
24. Desiraju, G. R. Hydrogen Bridges in Crystal Engineering: Interactions Without Borders. *Acc. Chem. Res.* **2002**, *35*, 565-573.
25. Choi, M.; Na, K.; Kim, J.; Sakamoto, Y.; Terasaki, O.; Ryoo, R., Stable single-unit-cell nanosheets of zeolite MFI as active and long-lived catalysts. *Nature* **2009**, *461* (7261), 246-9.
26. Li, X.; Xu, H.-S.; Leng, K.; Chee, S. W.; Zhao, X.; Jain, N.; Xu, H.; Qiao, J.; Gao, Q.; Park, I.-H.; Quek, S. Y.; Mirsaidov, U.; Loh, K. P., Partitioning the interlayer space of covalent organic frameworks by embedding pseudorotaxanes in their backbones. *Nat. Chem.* **2020**, *12* (12), 1115-1122.
27. Marty, R.; Nigon, R.; Leite, D.; Frauenrath, H., Two-fold odd-even effect in self-assembled nanowires from oligopeptide-polymer-substituted perylene bisimides. *J. Am. Chem. Soc.* **2014**, *136* (10), 3919-27.
28. Thalladi, V. R.; Boese, R.; Weiss, H.-C., The Melting Point Alternation in  $\alpha,\omega$ -Alkanediols and  $\alpha,\omega$ -Alkanediamines: Interplay between Hydrogen Bonding and Hydrophobic Interactions. *Angew. Chem. Int. Ed.* **2000**, *39* (5), 918-922.
29. Zhao, C.; Lyu, H.; Ji, Z.; Zhu, C.; Yaghi, O. M., Ester-Linked Crystalline Covalent Organic Frameworks. *J. Am. Chem. Soc.* **2020**, *142* (34), 14450-14454.
30. Peng, Y.; Li, L.; Zhu, C.; Chen, B.; Zhao, M.; Zhang, Z.; Lai, Z.; Zhang, X.; Tan, C.; Han, Y.; Zhu, Y.; Zhang, H., Intramolecular Hydrogen Bonding-Based Topology Regulation of Two-Dimensional Covalent Organic Frameworks. *J. Am. Chem. Soc.* **2020**, *142* (30), 13162-13169.
31. Iijima, S., Helical microtubules of graphitic carbon. *Nature* **1991**, *354* (6348), 56-58.
32. Shimada, N.; Kinoshita, H.; Umegae, T.; Azumai, S.; Kume, N.; Ochiai, T.; Takenaka, T.; Sakamoto, W.; Yamada, T.; Furuta, T.; Masuda, T.; Sakurai, M.; Higuchi, H.; Maruyama, A., Cationic Copolymer-Chaperoned 2D-3D Reversible Conversion of Lipid Membranes. *Adv. Mater.* **2019**, *31* (44), e1904032.

# Table of contents

- Bottom up synthesis of crystalline COFs
- Template-free synthesis of porous nanotubes
- Covalent Organic Framework with Flexible linkers
- Odd-even effects on frameworks.



**Even Linkers**

**Odd Linkers**

